# Supporting Information for

## Na/Ca Intermixing around Silicate and Phosphate Groups in Bioactive Phosphosilicate Glasses Revealed by Heteronuclear Solid-State NMR and Molecular Dynamics Simulations

Renny Mathew, Baltzar Stevensson, and Mattias Edén*

Physical Chemistry Division, Department of Materials and Environmental Chemistry, Arrhenius Laboratory, Stockholm University, SE-106 91 Stockholm, Sweden

*Corresponding author. E-mail: *mattias.eden@mmk.su.se*

## Contents

# S1 Experimental and Numerical Procedures

## S1.1 MD Simulations

The MD simulation procedures followed those outlined in our previous work.[S1–S3] Except for the glass models of the $CaO$–$SiO_2$ and $Na_2O$–$SiO_2$–$P_2O_5$ glasses presented herein, the parameters utilized for all simulations of the $Na_2O$–$CaO$–$SiO_2$–$P_2O_5$ glasses were discussed by Stevensson *et al.*[S2] **Table S2** lists the number of simulated atoms, box dimensions, as well as the number of independent simulations performed for each glass composition.

The polarizable shell-model potential utilized cations carrying their full formal charges, whereas the $O^{2-}$ species were represented by core ($O_C$) and shell ($O_S$) units with charges of $z_C = +0.8482e$ and $z_S = -2.8482e$, respectively, implying $z_C + z_S = -2$.[S4] They were coupled by a 300 THz harmonic oscillator. A Buckingham potential accounted for all short-range $O_S$–$O_S$ and cation–$O_S$ pair interactions [using the parameters of refs. (S5–S7)], which were evaluated out to 0.8 nm.[S4] Long-range Coulombic interactions were calculated by a smoothed particle mesh Ewald summation[S8] with a 1.2 nm real-space cut-off and an accuracy of $10^{-6}$. The O–Si–O and O–P–O intratetrahedral angles were constrained with three-body truncated harmonic potentials.[S8] The equations of motion were integrated in steps of 0.2 fs using the velocity Verlet integrator, while the temperature was controlled by a Berendsen thermostat associated with a 1.0 ps time constant.

## S1.2 Heteronuclear NMR Experimentation

Here we provide the experimental details of the heteronuclear $^{23}Na \longleftrightarrow {}^{29}Si$ and $^{23}Na \longleftrightarrow {}^{31}P$ NMR experimentation. For the $^{23}Na$–$^{31}P$ pair, $M_2$(P–Na) and $M_2$(Na–P) data were reported by Stevensson *et al.*[S3] for several $BG_p^q(\overline{N}_{BO}^{Si})$ samples. Ref. (S3) reported a straightforward $M_2$(S–I)$\longleftrightarrow$ $M_2$(I–S) conversion protocol (demonstrated on the $^{23}Na$–$^{31}P$ pair in phosphosilicate glasses), whereas the present study discusses the implications for composition/structure correlations, as well as presenting new data from additional glass specimens.

All $^{23}Na\{^{31}P\}$ REDOR and $^{31}P\{^{23}Na\}$ REAPDOR NMR data discussed in the main text were recorded at 9.4 T and 14.000 kHz MAS with a Bruker Avance-III spectrometer and a 4 mm triple-resonance (TR) MAS probehead. The spinning rate was stable within ±2 Hz throughout. All recoupling experiments involved central-transition (CT) selective $^{23}Na$ pulses operating at $\nu_1^{Na,CT} \approx 16.0$ kHz, corresponding to 90°/180° pulse-lengths of 15.6/31.3 $\mu$s. The $^{31}P/^{29}Si$ 180° recoupling pulses were 6.9/8.0 $\mu$s for both REDOR and REAPDOR NMR acquisitions, with the rf phases cycled according to XY16 scheme[S9] to minimize radio-frequency (rf) errors. The dipolar dephasing data was sampled at *even integral* multiples of the rotational period $\tau_r$. The REAPDOR experiments started from directly excited $^{31}P/^{29}Si$ magnetization by application of a 90° pulse. The adiabatic-passage pulse for REAPDOR operated at $\nu_1^{Na} = 75$ kHz for 24 $\mu$s (i.e., $\tau_r/3$). Saturation-recovery blocks were used prior to relaxation delays of 20 s and 200 s in the recording of each $^{31}P\{^{23}Na\}$ and $^{29}Si\{^{23}Na\}$ REAPDOR signal transient, respectively, whereas those for $^{23}Na\{^{31}P\}$ and $^{23}Na\{^{29}Si\}$ REDOR employed 4 s. All REDOR experimentation utilized the RAPT technique[S10] to enhance the $^{23}Na$ CT magnetization and thereby the experimental sensitivity, where typically 40 pulse-blocks were employed with equal pulse/interpulse durations of 0.55 $\mu$s and $\nu_1^{Na}$ =75 kHz.

The REDOR/REAPDOR NMR data were acquired in 3–4 blocks per phosphosilicate sample, each involving 16–64 accumulated signal transients, depending on the particular experimental protocol and glass composition. These independent experimental data sets were separately processed, integrated, and numerically fitted to eq. (2), as discussed in detail in the **SI** of Stevensson *et al.*[S3] Note that all heteronuclear NMR experimentation involved full rotors. The presence of rf

inhomogeneity is known to give underestimated dipolar-deriving structural data.[S11,S12] **Table S4** reports the resulting average dipolar second moments and their associated uncertainties, as obtained from the blocks of independently acquired experimental data. All experiments were performed at 25 °C. To verify if Na mobility could affect the dipolar dephasing, we also performed $^{29}$Si{$^{23}$Na} REAPDOR experiments at −80 °C on the $BG^{1.00}_{6.0}(2.5)$ specimen, however, without observing any significant difference.

Note that computer modeling was used exclusively to probe the Ca–Si/P spatial proximities, owing to the very low natural abundance (0.15%) and substantial costs of the $^{43}$Ca isotope ($S$=7/2), coupled with its low NMR signal-sensitivity even for enriched specimens.

## S2 The Relative Dephasing for $^{29}$Si⟷$^{23}$Na and $^{31}$P⟷$^{23}$Na in REDOR/REAPDOR NMR

It is instructive to compare the different time-scales over which the $^{23}$Na⟷$^{31}$P and $^{23}$Na⟷$^{29}$Si experiments dephase in Figs. **4** and **6** in relation to both the Si and P contents of the BG and the very different sizes of the magnetogyric ratios ($\gamma_{Si} = -5.3{\cdot}10^7$ rads$^{-1}$T$^{-1}$; $\gamma_P = 10.8{\cdot}10^7$ rads$^{-1}$T$^{-1}$) that together with the common factor $\gamma_{Na} = 7.1{\cdot}10^7$ rads$^{-1}$T$^{-1}$ for $^{23}$Na enter the expressions for the respective dipolar coupling constants $b_{Na-Si}$ and $b_{Na-P}$. The ratio $|\gamma_P/\gamma_{Si}| \approx 2$ implies that if the number-densities of $^{29}$Si and $^{31}$P would be identical in the glass (note that $r_{Si-Na} \approx r_{P-Na}$), the stronger $^{23}$Na–$^{31}$P dipolar contacts themselves should lead to roughly $(\gamma_P/\gamma_{Si})^2 \approx 4$ times faster $^{23}$Na{$^{31}$P} REDOR dephasing compared to its $^{23}$Na{$^{29}$Si} counterpart [see eq. (1)]. Yet, the significantly higher Si content relative to that of P in the present glasses counterbalance the effect of the larger $\gamma_P$ value: this yields a comparable $^{23}$Na{$^{29}$Si} dephasing for the $^{29}$Si-enriched $BG^{0.43}_{6.0}(2.5)$ and $BG^{1.00}_{6.0}(2.5)$ glasses [Fig. **6**(a)] relative to that of the $^{23}$Na{$^{31}$P} REDOR scenario shown in Fig. **4**(a). For the REAPDOR experimentation, on the other hand, where all concentration effects of the *observed* $^{31}$P of $^{29}$Si species are eliminated [see eq. (1)], the consequences from the widely differing magnetogyric ratios ($\gamma_P$ and $\gamma_{Si}$) become evident; they account for the markedly slower $^{29}$Si{$^{23}$Na} REAPDOR dynamics observed in Fig. **6** compared with the $^{31}$P{$^{23}$Na} counterpart in Fig. **4**. The relative dephasing trends among the $^{29}$Si/$^{23}$Na and $^{31}$P/$^{23}$Na pairs of nuclei are mirrored in the respective NMR/MD-derived second moments listed in **Table S4**, where $M_2$(Na–P) and $M_2$(Na–Si) reveal similarly-sized values, whereas the $M_2$(P–Na) data are almost an order of magnitude larger than those of $M_2$(Si–Na).

The slower dipolar recoupling dynamics of the $^{29}$Si{$^{23}$Na} REAPDOR experimentation and its concurrent accumulation of rf-pulse errors account for the strongly non-ideal dephasing behavior observed beyond a few ms; note that in the case of REAPDOR, the train of 180° pulses is applied to the *observed* $^{29}$Si spins (see Fig. **S1**). Moreover, the REAPDOR technique is well-known to be very susceptible to MAS-rate fluctuations.[S13,S14] The best-fit $M_2$(Si–Na) value from the mixed-modifier glass $BG^{0.43}_{6.0}(2.5)$ accorded very well with that obtained by MD simulations. In contrast, the second moment measured directly by $^{29}$Si{$^{23}$Na} REAPDOR from the Na–Si–P–O glass $BG^{1.00}_{6.0}(2.5)$ is significantly lower than its modeled counterpart, while that determined indirectly by converting the corresponding $^{23}$Na{$^{29}$Si} REDOR-derived result accorded well with the MD result. We have no satisfactory explanation for these observations, but we note that Na mobility (which is well-known to affect dipolar-coupling-based experiments) is unlikely to be the reason, given that no significant differences were observed in the $^{29}$Si{$^{23}$Na} NMR signal dephasing between experiments performed at room temperature and at −80 °C under otherwise identical conditions.

## S3 Prediction of $Z^T_{\mathbf{tot}}$ for each $Q^n_{\mathbf{Si}}$ and $Q^n_{\mathbf{P}}$ Group

The MD-derived total coordination number $Z_{\mathrm{tot}}(Q^n_T) \equiv Z(Q^n_T{-}\mathrm{Na}) + Z(Q^n_T{-}\mathrm{Ca})$ of each $Q^n_T$ moiety depends foremost on the total number density of the modifier ions, $\rho(M_{\mathrm{tot}})$. For the phosphate species, good fits were obtained by using this parameter alone,

$$Z_{\mathrm{tot}}(Q^0_{\mathrm{P}}) = 6.0281 + 0.1992\rho(M_{\mathrm{tot}}), \qquad R^2 = 0.970, \tag{S1}$$

$$Z_{\mathrm{tot}}(Q^1_{\mathrm{P}}) = 3.8893 + 0.2259\rho(M_{\mathrm{tot}}), \qquad R^2 = 0.965, \tag{S2}$$

whereas the coordination numbers of each $Q^n_{\mathrm{Si}}$ species generally also depended on the P content (i.e., $\rho_{\mathrm{P}}$), as follows:

$$Z_{\mathrm{tot}}(Q^1_{\mathrm{Si}}) = 5.7693 + 0.1741\rho(M_{\mathrm{tot}}), \qquad R^2 = 0.928, \tag{S3}$$

$$Z_{\mathrm{tot}}(Q^2_{\mathrm{Si}}) = 3.3472 + 0.2219\rho(M_{\mathrm{tot}}) - 0.0617\rho_{\mathrm{P}}, \qquad R^2 = 0.996, \tag{S4}$$

$$Z_{\mathrm{tot}}(Q^3_{\mathrm{Si}}) = 1.1667 + 0.2495\rho(M_{\mathrm{tot}}) - 0.0853\rho_{\mathrm{P}}, \qquad R^2 = 0.998, \tag{S5}$$

$$Z_{\mathrm{tot}}(Q^4_{\mathrm{Si}}) = -0.7018 + 0.2471\rho(M_{\mathrm{tot}}), \qquad R^2 = 0.962. \tag{S6}$$

Note that the best-fit coefficient for $\rho_{\mathrm{P}}$ is zero for the $Q^1_{\mathrm{Si}}$ groups (i.e., $Z_{\mathrm{tot}}(Q^1_{\mathrm{Si}})$ is independent on $\rho_{\mathrm{P}}$), while *negative* coefficients are observed in the expressions for the $Q^2_{\mathrm{Si}}$ and $Q^3_{\mathrm{Si}}$ groups, where the *magnitude* of the coefficient increases together with the number of BO atoms ($n$) at the $Q^n_{\mathrm{Si}}$ tetrahedron. This trend reflects that the most negatively charged $Q^1_{\mathrm{Si}}$ groups ($\mathrm{SiO}^{3-}_{3.5}$) control their own coordination shells to a larger extent than their $Q^2_{\mathrm{Si}}$ ($\mathrm{SiO}^{2-}_3$) and $Q^3_{\mathrm{Si}}$ ($\mathrm{SiO}^{-}_{2.5}$) counterparts. Hence, the coordination numbers of the $Q^2_{\mathrm{Si}}$ and $Q^3_{\mathrm{Si}}$ groups *reduces* when the P content of the glass is increased, because the higher negative charge of the $Q^0_{\mathrm{P}}$ ($\mathrm{PO}^{3-}_4$) unit attract the $\mathrm{Na}^+/\mathrm{Ca}^{2+}$ cations more efficiently. In contrast, the formally *uncharged* $Q^4_{\mathrm{Si}}$ groups also give an exception in that $Z_{\mathrm{tot}}(Q^4_{\mathrm{Si}})$ is also independent on $\rho_{\mathrm{P}}$. The reason is likely their *overall* low affinity for the modifiers.

Figure **S3** plots the correlation between the MD-derived coordination number and its best-fit counterpart calculated from eqs. (S1)–(S6) for each $Q^n_T$ group. The agreement is very good throughout, as reflected in the near-unity correlation coefficients ($R^2 \approx 1$). The largest deviations ($R^2 = 0.928$) are observed for $Z_{\mathrm{tot}}(Q^1_{\mathrm{Si}})$. Note, however, that no quality-improvement of the fit [eq. (S3)] resulted when also invoking $\rho_{\mathrm{P}}$ as an independent parameter in the numerical fitting ($R^2 = 0.921$).

## S4 Contributions from the First Coordination Shell $Q^n_T$–$M$ Contacts to $M_2(Q^n_T$–$M)$

**Table S6** reveals that the Si/P–Na/Ca contacts in the first coordination shell of each $Q^n_T$ group generally contributes to 80–90% of the (converged) $M_2(Q^n_T$–Na) and $M_2(Q^n_T$–Ca) second moments. Noteworthy, these fractions are almost equal for Na and Ca and essentially independent on the glass composition, meaning that the conclusions about the relative $T$–Na and $T$–Ca preferences drawn from the $\{Z^T_{\mathrm{Na}}, Z^T_{\mathrm{Ca}}\}$ pair are fully representative also for the longer-range contacts. The only exceptions are the lower-charged silicate groups: the $\mathrm{Na}^+/\mathrm{Ca}^{2+}$ cations of the first coordination shell for $Q^3_{\mathrm{Si}}$ accounts for 81% (Na) and 73% (Ca) out of the respective total $M_2(Q^3_{\mathrm{Si}}$–$M)$ values, whereas the $Q^4_{\mathrm{Si}}$ groups reveal much lower fractions of ≈73% and ≈39% for Na and Ca, respectively (see **Table S6**). Consequently, assessments made from $\{Z^T_{\mathrm{Na}}, Z^T_{\mathrm{Ca}}\}$ data of these silicate groups tend

to overestimate their preferences for Na contacts; only slightly for the $Q^3_{\mathrm{Si}}$ moieties, but substantially for $Q^4_{\mathrm{Si}}$. These effects are apparent in the $R_{\mathrm{Na/Ca}}(Q^n_{\mathrm{Si}})$ factors listed in **Table S5**, whose values derived by requiring that Si and Na/Ca share O atoms (and thereby share first coordination shells) are larger than the $R_{\mathrm{Na/Ca}}(Q^n_T)$ counterpart evaluated out to $r$=450 pm. We stress, however, that the deviations among the two $R_{\mathrm{Na/Ca}}(Q^n_T)$ sets are insignificant for all other $Q^n_T$ species, which consistently reveal values well within the data uncertainties.

## S5 Limitations of Heteronuclear and $^{17}$O NMR Experimentation

While the experimental/numerical errors of the NMR/MD-stemming $M_2$(P–Na) values are generally within the symbol sizes in Figs. **5** and **10**(a), and the error bars of the various $\{P_{\mathrm{Ca}}\}$ estimates in Fig. **10**(b) do generally not overlap, the *spread* among the two independent experimental datasets better conveys the accuracy limited by *systematic* errors of this type of heteronuclear NMR implementations. As discussed further in refs. (S2,S3), $M_2$(S–I) data from glasses are prone to be *underestimated* due to rf inhomogeneity, the presence of paramagnetic doping, and the approximations inherent to eq. (2) used for fitting. Note that the second moments of Figs. **5** and **10** were already corrected for most of the these systematic errors; if the same analysis is applied to the *uncorrected* REAPDOR-stemming data,[S3] significantly higher $P_{\mathrm{Ca}}$-values between 0.33–0.46 results.

Furthermore, given that we are quantifying a degree of preference for Ca (i.e., $P_{\mathrm{Ca}}$) from information about $M_2$(P–Na), *any underestimate in* $M_2$(P–Na) *translates into an overestimate of* $P_{\mathrm{Ca}}$. This property follows from eqs. (6) and (7) and that only the factor $P_M$ of the *preferred* cation $M$ is well-defined (i.e., there is no exact relationship between $P_M$ and $P_{M'}$). An independent measurement of $M_2$(P–Ca) is unfortunately intractable (see **section S1.2**), but such values are *also* expected to be underestimated, thereby leading to an *under*estimation of $P_{\mathrm{Ca}}$. Thus, access to *both* independent $M_2$(P–Ca) and $M_2$(P–Na) results would provide both upper/lower limits of the $P_{\mathrm{Ca}}$ estimate. Moreover, the $M_2(Q^0_{\mathrm{P}}$–Na) values calculated from the $\{P_M,\, Z^T_{\mathrm{tot}}(Q^n_T),\, \overline{r}_{T-M}\}$ parameters are inherently biased to the MD-generated structural data from which they were derived. Higher experimental $P_{\mathrm{Ca}}$ parameters are therefore anticipated from the *lower* experimental $M_2$(P–Na) data relative to the simulated ones (Fig. **5**). The gray region around $P_{\mathrm{Ca}}$=$P_{\mathrm{Na}}$=0 in Fig. **10**(a) illustrates the spread in $M_2(Q^0_{\mathrm{P}}$–Na) resulting solely when $Z_{\mathrm{tot}}(Q^0_{\mathrm{P}})$ is varied by $\pm$1 (i.e., by $\approx$10%).

After the critical remarks on the present data, we note that our conclusions about modifier (dis)ordering in glasses are both more transparent and precise than previous assessments by similar heteronuclear recoupling experimentation applied to other glass systems/nuclei, where the conclusions from the second-moment data were of more qualitative nature.[S15–S22] Moreover, earlier inferences about cation intermixing around silicate groups by $^{17}$O NMR[S23–S25] are plagued by similar problems as the heteronuclear NMR experimentation: limited spectral resolution with overlap among the $^{17}$O resonances from distinct BO/NBO–$M/M'$ contacts and assumptions required about the total coordination number of modifiers at the O sites may together produce significant systematic errors in the subsequent NMR peak-deconvolution into several peaks of *a priori* unknown positions and widths.

**Table S1: Fractional Populations of $Q^n_P$ and $Q^n_{Si}$ Groups[a]**

| glass | P | | Si | | | | silicate network connectivity | | |
|---|---|---|---|---|---|---|---|---|---|
| | $x^0_P$ | $x^1_P$ | $x^1_{Si}$ | $x^2_{Si}$ | $x^3_{Si}$ | $x^4_{Si}$ | $\overline{N}^{Si}_{BO}$(nom) | $\overline{N}^{Si}_{BO}$(NMR) | $\overline{N}^{Si}_{BO}$(MD) |
| $BG^0_0(2.0)$ | – | – | 0.168(0.243) | 0.745(0.472) | 0.087(0.241) | 0.000(0.022) | 2.00 | 1.92 | 2.00 |
| $BG^{0.48}_{2.6}(2.1)$ | 0.959(0.834) | 0.041(0.166) | 0.066(0.186) | 0.724(0.517) | 0.210(0.266) | 0.000(0.021) | 2.11 | 2.14 | 2.10 |
| $BG^{0.41}_{6.0}(2.1)$ | 0.955(0.798) | 0.045(0.200) | 0.056(0.197) | 0.658(0.514) | 0.286(0.252) | 0.000(0.027) | 2.15 | 2.20 | 2.09 |
| $BG^0_0(2.5)$ | – | – | 0.036(0.080) | 0.417(0.415) | 0.520(0.414) | 0.027(0.088) | 2.50 | 2.54 | 2.50 |
| $BG^{0.43}_0(2.5)$ | – | – | 0.015(0.068) | 0.409(0.428) | 0.555(0.425) | 0.021(0.076) | 2.50 | 2.58 | 2.50 |
| $BG^{0.43}_{1.0}(2.5)$ | 0.899(0.670) | 0.101(0.318) | 0.017(0.073) | 0.455(0.426) | 0.512(0.435) | 0.016(0.065) | 2.50 | 2.53 | 2.49 |
| $BG^{0.43}_{2.0}(2.5)$ | 0.896(0.721) | 0.104(0.267) | 0.012(0.080) | 0.405(0.418) | 0.563(0.440) | 0.020(0.060) | 2.50 | 2.59 | 2.48 |
| $BG^{0.43}_{4.0}(2.5)$ | 0.931(0.622) | 0.069(0.364) | 0.010(0.084) | 0.372(0.443) | 0.598(0.409) | 0.020(0.063) | 2.50 | 2.63 | 2.45 |
| $BG^{0.43}_{6.0}(2.5)$ | 0.902(0.690) | 0.098(0.304) | 0.010(0.087) | 0.423(0.457) | 0.551(0.392) | 0.016(0.062) | 2.50 | 2.57 | 2.42 |
| $BG^{1.00}_{6.0}(2.5)$ | 0.975(0.735) | 0.025(0.263) | 0.013(0.071) | 0.430(0.465) | 0.549(0.417) | 0.008(0.046) | 2.50 | 2.55 | 2.44 |
| $BG^{0.48}_{2.6}(2.7)$ | 0.838(0.517) | 0.162(0.475) | 0.006(0.041) | 0.242(0.336) | 0.677(0.507) | 0.075(0.115) | 2.74 | 2.82 | 2.70 |
| $BG^{0.43}_0(2.9)$ | – | – | 0.000(0.016) | 0.094(0.225) | 0.793(0.571) | 0.113(0.189) | 2.93 | 3.02 | 2.93 |
| $BG^{0.43}_{2.0}(2.9)$ | 0.795(0.417) | 0.205(0.553) | 0.000(0.017) | 0.108(0.246) | 0.791(0.553) | 0.101(0.183) | 2.93 | 2.99 | 2.90 |
| $BG^{0.43}_{3.0}(2.9)$ | 0.814(0.444) | 0.186(0.528) | 0.000(0.020) | 0.144(0.252) | 0.779(0.562) | 0.077(0.166) | 2.93 | 2.93 | 2.87 |
| $BG^{0.43}_{4.0}(2.9)$ | 0.805(0.440) | 0.195(0.554) | 0.000(0.022) | 0.118(0.269) | 0.791(0.539) | 0.091(0.169) | 2.93 | 2.97 | 2.86 |
| $BG^{0.43}_{6.0}(2.9)$ | 0.821(0.460) | 0.179(0.517) | 0.000(0.028) | 0.121(0.290) | 0.778(0.539) | 0.101(0.143) | 2.93 | 2.98 | 2.80 |

[a]Left-most entries are $\{x^n_P, x^n_{Si}\}$ data extracted by deconvoluting MAS NMR spectra, as described in detail by Mathew *et al.*[S1] The values within parentheses are MD-derived populations. The various $\overline{N}^{Si}_{BO}$ data were calculated either from (*i*) the *nominal* value obtained from the oxide equivalents presented in **Table 1** and *assuming* that the entire phosphate speciation consists of orthophosphate groups [$\overline{N}^{Si}_{BO}$(nom); see ref. (S1) for details], or from (*ii*) the $\{x^n_{Si}\}$ set obtained by NMR [$\overline{N}^{Si}_{BO}$(NMR)] or (*iii*) by MD simulations [$\overline{N}^{Si}_{BO}$(MD)]. While the NMR/MD-derived data generally accord well, we refer to Mathew *et al.*[S1] for additional information and discussion about the reasons behind the discrepancies in the various $\{x^n_T\}$ and $\overline{N}^{Si}_{BO}$ results. Any deviation to unity for the sum over each MD-derived phosphate $\{x^n_P\}$ or silicate $\{x^n_{Si}\}$ set reflects the presence of minor $x^2_P$ or $x^0_{Si}$ populations.

**Table S2: Molecular Dynamics Simulation Parameters**[a]

| glass | $N_{\mathrm{tot}}$ | $N_{\mathrm{Na}}$ | $N_{\mathrm{Ca}}$ | $N_{\mathrm{P}}$ | $N_{\mathrm{Si}}$ | $N_{\mathrm{sim}}$ | $a$/nm[b] |
|---|---|---|---|---|---|---|---|
| $\mathrm{BG}_{0}^{0}(2.0)$ | 6000 | 0 | 1200 | 0 | 1200 | 2 | 4.309 |
| $\mathrm{BG}_{2.6}^{0.48}(2.1)$ | 10017 | 1718 | 950 | 184 | 1632 | 2 | 5.114 |
| $\mathrm{BG}_{6.0}^{0.41}(2.1)$ | 6123 | 928 | 681 | 252 | 829 | 2 | 4.336 |
| $\mathrm{BG}_{0}^{0}(2.5)$ | 5787 | 0 | 963 | 0 | 1287 | 2 | 4.262 |
| $\mathrm{BG}_{0}^{0.43}(2.5)$ | 5516 | 744 | 484 | 0 | 1144 | 2 | 4.196 |
| $\mathrm{BG}_{1.0}^{0.43}(2.5)$ | 12279 | 1686 | 1097 | 88 | 2416 | 4 | 5.473 |
| $\mathrm{BG}_{2.0}^{0.43}(2.5)$ | 5768 | 808 | 524 | 80 | 1076 | 3 | 4.257 |
| $\mathrm{BG}_{4.0}^{0.43}(2.5)$ | 6280 | 904 | 588 | 176 | 1044 | 4 | 4.379 |
| $\mathrm{BG}_{6.0}^{0.43}(2.5)$ | 5644 | 840 | 544 | 232 | 828 | 2 | 4.223 |
| $\mathrm{BG}_{6.0}^{1.00}(2.5)$ | 6188 | 1928 | 0 | 232 | 828 | 2 | 4.430 |
| $\mathrm{BG}_{2.6}^{0.48}(2.7)$ | 9999 | 1400 | 771 | 180 | 1909 | 2 | 5.129 |
| $\mathrm{BG}_{0}^{0.43}(2.9)$ | 5606 | 604 | 394 | 0 | 1304 | 2 | 4.238 |
| $\mathrm{BG}_{2.0}^{0.43}(2.9)$ | 6080 | 696 | 456 | 88 | 1272 | 3 | 4.347 |
| $\mathrm{BG}_{3.0}^{0.43}(2.9)$ | 6081 | 722 | 471 | 126 | 1205 | 2 | 4.350 |
| $\mathrm{BG}_{4.0}^{0.43}(2.9)$ | 6372 | 776 | 508 | 176 | 1192 | 4 | 4.414 |
| $\mathrm{BG}_{6.0}^{0.43}(2.9)$ | 6000 | 776 | 504 | 240 | 996 | 2 | 4.320 |

[a] $N_{\mathrm{tot}}$ represents the total number of atoms in the simulation of one glass model, whereas $\{N_{\mathrm{Na}}$, $N_{\mathrm{Ca}}$, $N_{\mathrm{P}}$, $N_{\mathrm{Si}}\}$ correspond to those of {Na, Ca, P, Si}, respectively, and $N_{\mathrm{sim}}$ is the number of independent glass models generated.

[b] Side length of the cubic box.

**Table S3: $^{23}$Na NMR parameters[a]**

| glass | $\delta_{\mathrm{Na}}^{\mathrm{CG}}$ (ppm) | fwhm (ppm) | $\overline{\delta}_{\mathrm{Na}}^{\mathrm{iso}}$ (ppm) | $\overline{C}_{Q\eta}$ (MHz) | $W_{\mathrm{Na}}^{\mathrm{iso}}$ (ppm) |
|---|---|---|---|---|---|
| $BG_{2.6}^{0.48}(2.1)$ | −2.5 | 25.3 | 8.0 | 3.50 | 19.7 |
| $BG_{6.0}^{0.41}(2.1)$ | −2.9 | 24.7 | 7.4 | 3.51 | 18.7 |
| $BG_{0}^{0.43}(2.5)$ | −5.9 | 26.3 | 3.6 | 3.61 | 20.1 |
| $BG_{2.0}^{0.43}(2.5)$ | −5.3 | 25.8 | 4.2 | 3.61 | 19.2 |
| $BG_{4.0}^{0.43}(2.5)$ | −5.1 | 25.2 | 4.2 | 3.61 | 18.8 |
| $BG_{6.0}^{0.43}(2.5)$ | −4.7 | 24.7 | 5.1 | 3.47 | 18.8 |
| | −18.0[b] | 38.7[b] | 5.0[b] | 3.65[b] | 18.9[b] |
| $BG_{6.0}^{1.00}(2.5)$ | 0.9 | 19.4 | 9.5 | 3.42 | 14.1 |
| $BG_{2.6}^{0.48}(2.7)$ | −7.2 | 25.4 | 2.9 | 3.57 | 18.9 |
| $BG_{0}^{0.43}(2.9)$ | −9.4 | 25.4 | 0.2 | 3.57 | 19.0 |
| | −22.8[b] | 39.8[b] | −0.4[b] | 3.60[b] | 20.8[b] |
| $BG_{2.0}^{0.43}(2.9)$ | −8.9 | 25.2 | 0.7 | 3.58 | 18.8 |
| $BG_{4.0}^{0.43}(2.9)$ | −8.2 | 25.1 | 1.6 | 3.55 | 18.8 |

[a]Center-of-gravity shift ($\delta_{\mathrm{Na}}^{\mathrm{CG}}$; uncertainty ±0.1 ppm) and full-width at half maximum (fwhm; ±0.2 ppm) of the $^{23}$Na MAS NMR peak recorded at $B_0 = 14.1$ T. The remaining data are best-fit parameters extracted from numerical simulations, assuming a single $^{23}$Na site with a Gaussian distribution of isotropic chemical shifts ($\delta_{\mathrm{Na}}^{\mathrm{iso}}$) and a Czjzek distribution[S26] of quadrupolar products ($C_{Q\eta}$): $^{23}$Na average quadrupolar product $\left(\overline{C}_{Q\eta}\right)$, average isotropic chemical shift ($\overline{\delta}_{\mathrm{Na}}^{\mathrm{iso}}$; ±1 ppm) and the shift-distribution width ($W_{\mathrm{Na}}^{\mathrm{iso}}$; ±2 ppm). Owing to the significant $\overline{C}_{Q\eta}/W_{\mathrm{Na}}^{\mathrm{iso}}$ interdependence, where both parameters cause resonance-broadening, the $\overline{C}_{Q\eta}$-values were first determined by simultaneously fitting the two sets of NMR spectra from $BG_{0}^{0.43}(2.9)$ and $BG_{6.0}^{0.43}(2.5)$ that were recorded at both 14.1 T and 9.4 T (where the latter field provides more reliable $\overline{C}_{Q\eta}$-values). We note that the value $\overline{C}_{Q\eta} \approx 1.6$ MHz stated previously in ref. (S3) as representative for the present glasses should be scaled by the factor $\sqrt{5}$.

[b]Results obtained at $B_0 = 9.4$ T.

**Table S4: MD and NMR Derived Dipolar Second Moments[a]**

| glass | $M_2^{MD}$(Na–P)—$M_2^{NMR}$(Na–P) $10^4$ Hz$^2$ | $M_2^{MD}$(P–Na)—$M_2^{NMR}$(P–Na)[b] $10^5$ Hz$^2$ | $M_2^{MD}$(Na–Si) $10^4$ Hz$^2$ | $M_2^{MD}$(Si–Na)[c] $10^5$ Hz$^2$ |
|---|---|---|---|---|
| $BG_{2.6}^{0.48}$(2.1) | 2.05±0.15—2.18±0.01 | 9.57±0.28—9.20±0.12(10.22±0.04) | 3.25±0.01 | 1.71±0.01 |
| $BG_{6.0}^{0.41}$(2.1) | 4.64±0.07—4.49±0.02 | 8.54±0.05—7.55±0.10(8.26±0.04) | 2.61±0.04 | 1.46±0.03 |
| $BG_{0}^{0.43}$(2.5) | — | — | 4.04±0.04 | 1.31±0.01 |
| $BG_{1.0}^{0.43}$(2.5) | 0.83±0.39 | 7.90±0.25 | 3.81±0.01 | 1.33±0.01 |
| $BG_{2.0}^{0.43}$(2.5) | 1.60±0.20—1.59±0.02 | 8.10±0.05—7.49±0.10(7.86±0.09) | 3.56±0.03 | 1.34±0.01 |
| $BG_{4.0}^{0.43}$(2.5) | 3.13±0.10—2.95±0.04 | 8.05±0.10—6.94±0.10(7.68±0.11) | 3.13±0.02 | 1.36±0.01 |
| $BG_{6.0}^{0.43}$(2.5) | 4.58±0.07—4.36±0.05 | 8.29±0.33—7.24±0.28(7.99±0.08) | 2.67±0.05(2.90±0.04)[e] | 1.36±0.03(1.43±0.03—1.49±0.02) |
| $BG_{6.0}^{1.00}$(2.5) | 4.01±0.07—5.45±0.01(4.07±0.05)[d] | 16.64±0.12—16.91±0.19(22.63±0.04) | 2.39±0.03(2.14±0.06)[e] | 2.78±0.01(1.90±0.01—2.60±0.03) |
| $BG_{2.6}^{0.48}$(2.7) | 2.03±0.16—1.92±0.02 | 7.90±0.24—7.44±0.10(7.44±0.07) | 3.44±0.01 | 1.26±0.01 |
| $BG_{0}^{0.43}$(2.9) | — | — | 4.17±0.02 | 0.97±0.01 |
| $BG_{2.0}^{0.43}$(2.9) | 1.74±0.19—1.40±0.03 | 6.86±0.31—6.11±0.10(5.77±0.12) | 3.68±0.05 | 1.01±0.01 |
| $BG_{3.0}^{0.43}$(2.9) | 2.42±0.14 | 6.95±0.15 | 3.47±0.01 | 1.04±0.01 |
| $BG_{4.0}^{0.43}$(2.9) | 3.12±0.10—2.79±0.03 | 6.87±0.09—6.27±0.21(6.23±0.07) | 3.25±0.02 | 1.06±0.01 |
| $BG_{6.0}^{0.43}$(2.9) | 4.46±0.07 | 7.21±0.04 | 2.83±0.03 | 1.10±0.01 |

[a]Dipolar second moments obtained from MD simulations [$M_2^{MD}$(S–I)] or S{I} REDOR/REAPDOR NMR [$M_2^{NMR}$(S–I)]. All experimental data were corrected as described by Stevensson *et al.*[S3]

[b]Values in parentheses were calculated from the corresponding $M_2^{NMR}$(Na–P) data obtained by $^{23}$Na{P} REDOR NMR by using the conversion $M_2$(P–Na)=$5x_{Na}M_2$(Na–P)$/x_P$.[S3]

[c]Values (a—b) in parentheses correspond to directly measured $M_2^{NMR}$(Si–Na) data from $^{29}$Si{$^{23}$Na} REAPDOR NMR experiments (left entry), whereas the right entry was derived from the corresponding $^{23}$Na{$^{29}$Si} REDOR NMR data.

[d]Derived from the $M_2^{NMR}$(P–Na) value of column 3.

[e]Experimental $M_2^{NMR}$(Na–Si) data in parentheses.

**Table S5: Relative Propensities of $SiO_4$ and $PO_4$ Groups to Coordinate Na and Ca[a]**

| glass | P | $Q^0_P$ | $Q^1_P$ | Si | $Q^1_{Si}$ | $Q^2_{Si}$ | $Q^3_{Si}$ | $Q^4_{Si}$ |
|---|---|---|---|---|---|---|---|---|
| $BG^{0.48}_{2.6}(2.1)$ | 0.93(0.91) | 0.89(0.88) | 1.14(1.15) | 0.94(0.93) | 0.75(0.73) | 0.94(0.92) | 1.21(1.27) | 1.48(2.26) |
| $BG^{0.41}_{6.0}(2.1)$ | 0.96(0.95) | 0.92(0.91) | 1.20(1.19) | 0.90(0.90) | 0.72(0.71) | 0.90(0.89) | 1.12(1.20) | 1.65(2.14) |
| $BG^{0.43}_{0}(2.5)$ | | | | 1.00(1.00) | 0.66(0.64) | 0.88(0.86) | 1.20(1.26) | 1.81(2.85) |
| $BG^{0.43}_{1.0}(2.5)$ | 0.89(0.89) | 0.83(0.83) | 1.07(1.07) | 1.00(1.00) | 0.67(0.64) | 0.88(0.87) | 1.20(1.26) | 1.75(2.48) |
| $BG^{0.43}_{2.0}(2.5)$ | 0.92(0.91) | 0.85(0.84) | 1.15(1.14) | 0.99(0.99) | 0.66(0.64) | 0.91(0.89) | 1.16(1.22) | 1.70(2.68) |
| $BG^{0.43}_{4.0}(2.5)$ | 0.92(0.91) | 0.86(0.85) | 1.05(1.04) | 0.98(0.97) | 0.72(0.70) | 0.87(0.85) | 1.17(1.22) | 1.79(2.65) |
| $BG^{0.43}_{6.0}(2.5)$ | 0.90(0.89) | 0.85(0.84) | 1.07(1.07) | 0.97(0.96) | 0.69(0.68) | 0.86(0.83) | 1.20(1.25) | 1.79(2.50) |
| $BG^{0.48}_{2.6}(2.7)$ | 0.88(0.87) | 0.80(0.79) | 0.99(0.99) | 1.02(1.01) | 0.61(0.60) | 0.85(0.82) | 1.15(1.19) | 2.02(3.02) |
| $BG^{0.43}_{0}(2.9)$ | | | | 1.05(1.05) | 0.56(0.54) | 0.79(0.76) | 1.12(1.13) | 1.66(2.58) |
| $BG^{0.43}_{2.0}(2.9)$ | 0.90(0.90) | 0.74(0.74) | 1.07(1.08) | 1.03(1.04) | 0.59(0.57) | 0.81(0.78) | 1.09(1.12) | 1.77(2.62) |
| $BG^{0.43}_{3.0}(2.9)$ | 0.88(0.87) | 0.74(0.73) | 1.05(1.03) | 1.04(1.04) | 0.59(0.57) | 0.76(0.74) | 1.16(1.18) | 1.76(2.52) |
| $BG^{0.43}_{4.0}(2.9)$ | 0.88(0.88) | 0.75(0.74) | 1.04(1.02) | 1.04(1.04) | 0.61(0.59) | 0.79(0.77) | 1.15(1.17) | 1.84(2.70) |
| $BG^{0.43}_{6.0}(2.9)$ | 0.93(0.89) | 0.81(0.81) | 1.06(0.98) | 1.01(1.02) | 0.65(0.59) | 0.78(0.77) | 1.10(1.16) | 1.81(2.72) |

[a]The left entries correspond to $R_{Na/Ca}(Q^n_T) = x_{Ca}Z(Q^n_T\text{–Na})/[x_{Na}Z(Q^n_T\text{–Ca})]$ with $T$={P, Si} evaluated for the cutoff radius $r$=450 pm. Values within parentheses represent $R_{Na/Ca}(Q^n_T)$ data calculated from coordination numbers derived by requiring *shared* oxygen species between {Si, P} and {Na, Ca}, i.e., the values representative for the first coordination shell of the $Q^n_T$ group and plotted in Fig. **7**. The labels "P" and "Si" correspond to the net results from the *total* $\{Q^n_P\}$ and $\{Q^n_{Si}\}$ speciations, respectively. The respective uncertainties ($\sigma$) are as follows: P($\pm$0.05); $Q^0_P$($\pm$0.04); $Q^1_P$($\pm$0.085); Si($\pm$0.015); $Q^1_{Si}$($\pm$0.05); $Q^2_{Si}$($\pm$0.02); $Q^3_{Si}$($\pm$0.03); $Q^4_{Si}$($\pm$0.15).

**Table S6: Parameters for Calculating $M_2(Q_T^n\text{–}M)$[a]**

| group | $\overline{r}_{T\text{–Na}}$ (pm) | $\overline{r}_{T\text{–Ca}}$ (pm) | $M_2^{\mathrm{FCS}}(Q_T^n\text{–Na})/M_2^{\mathrm{conv}}$ | $M_2^{\mathrm{FCS}}(Q_T^n\text{–Ca})/M_2^{\mathrm{conv}}$ |
|---|---|---|---|---|
| $Q_{\mathrm{P}}^0$ | 324 | 345 | 0.92(0.016) | 0.92(0.028) |
| $Q_{\mathrm{P}}^1$ | 328 | 352 | 0.90(0.034) | 0.86(0.055) |
| $Q_{\mathrm{Si}}^1$ | 325 | 344 | 0.90(0.016) | 0.92(0.038) |
| $Q_{\mathrm{Si}}^2$ | 330 | 349 | 0.87(0.020) | 0.86(0.046) |
| $Q_{\mathrm{Si}}^3$ | 336 | 354 | 0.81(0.014) | 0.73(0.049) |
| $Q_{\mathrm{Si}}^4$ | 343 | 371 | 0.73(0.036) | 0.39(0.096) |

[a]Average distance from the central atom (Si or P) of the $Q_T^n$ moiety to each of Na and Ca in the first coordination sphere (FCS) of the $Q_T^n$ group, i.e., second coordination sphere of Si and P. The ratio $M_2^{\mathrm{FCS}}(Q_T^n\text{–Na})/M_2^{\mathrm{conv}}$ represents the fraction of the *converged* dipolar second moment that the FCS accounts for. The data are presented as $M(S)$, with $M$ being the average value across the set of 13 mixed-modifier glasses (see **Table 1**). The span $S$ corresponds to the difference between the extreme values observed for the given $Q_T^n$ group among the glasses.

**Table S7: Distribution of Na and Ca around BO/NBO Sites in Soda-Lime-Silicate Glasses[a]**

| glass | $x$(NBO–Na) | $x$(NBO–Ca) | $x$(NBO–Na/Ca) | $Z$(NBO–$M_{\rm tot}$) |
|---|---|---|---|---|
| $BG_0^{0.43}(2.5)$ | 0.096(0.229) | 0.135(0.072) | 0.769(0.699) | 3.07 |
| $BG_0^{0.43}(2.9)$ | 0.109(0.267) | 0.177(0.096) | 0.712(0.635) | 2.74 |
| | 0.222[b] | 0.061[b] | 0.716[b] | |
| $BG_0^{0.5}(2.67)$[c] | 0.145(0.319) | 0.093(0.049) | 0.762(0.632) | |
| $BG_0^{0.5}(3.33)$[d] | 0.128(0.326) | — | — | |
| | 0.296[e] | 0.037[e] | 0.667[e] | |
| glass[f] | $x$(BO–Na) | $x$(BO–Ca) | $x$(BO–Na/Ca) | $Z$(BO–$M_{\rm tot}$) |
| $BG_0^{0.43}(2.5)$ | 0.645(0.440) | 0.126(0.252) | 0.127(0.206) | 1.35 |
| $BG_0^{0.43}(2.9)$ | 0.572(0.407) | 0.125(0.247) | 0.067(0.109) | 1.00 |
| | 0.606[g] | 0.394[g] | 0 | |
| $BG_0^{0.5}(2.67)$[c] | 0.710(0.516) | 0.111(0.211) | 0.087(0.181) | |
| | 0.667[h] | 0.333[h] | 0 | |

[a]MD-derived fractional populations $x(X\text{–Na})$, $x(X\text{–Ca})$, and $x(X\text{–Na/Ca})$ for $X = \{\text{BO, NBO}\}$. The uncertainties of each BO/NBO population of $BG_0^{0.43}(2.5)$ or $BG_0^{0.43}(2.9)$ is $\pm 0.01$ throughout. The NBO and BO average total coordination numbers with respect to *both* Na and Ca are listed in the rightmost column. However, $Z_{\rm tot} \equiv Z(X\text{–}M_{\rm tot})$ varies among different $X$=NBO or $X$=BO sites in the structure and this distribution also depends on the glass composition. Values within parentheses correspond to the respective populations obtained from a random Na/Ca partitioning for the given fraction $q = n(\text{Na}_2\text{O})/[n(\text{Na}_2\text{O}) + n(\text{CaO})]$ of the $BG_p^q(\overline{N}_{\rm BO}^{\rm Si})$ glass; they were obtained as a weighted average over a set of binomial distributions $\{B(\mathcal{Z}, q)\}$ (see Pedone *et al.*[S27]). Here the total coordination number $\mathcal{Z}_j$ of the oxygen site $j$ relates to $Z_{\rm tot}$ as $Z_{\rm tot} = \sum_j y_j \mathcal{Z}_j$ with $\sum_j y_j = 1$.

[b]Populations obtained from a single binomial distribution $B(\mathcal{Z}, q) = \mathcal{Z}![p!(\mathcal{Z}-p)!]^{-1} A^p (1-A)^{\mathcal{Z}-p}$ with $A = 2q/(1+q)$, $\mathcal{Z} = 3$, and $q = 0.43$.

[c]Data taken from Pedone *et al.*[S27]

[d]Data obtained by Lee and Stebbins from analysis of $^{17}$O MAS NMR spectra.[S24] An independent 3QMAS $^{17}$O NMR-derived estimate resulted in $x$(NBO–Na)=0.182. The value in parentheses corresponds to the prediction from a binomial distribution with $\mathcal{Z} = 3$ and $q = 0.5$;[S24] for unknown reasons, this value deviates slightly from that obtained by us (0.296).

[e]As in **b**, with $\mathcal{Z} = 3$ and $q = 0.5$.

[f]The fractional populations do not sum to unity because some BO sites do not coordinate to *any* network-modifier; these fractions amount to 0.102, 0.236, and 0.092 for the $BG_0^{0.43}(2.5)$, $BG_0^{0.43}(2.9)$, and $BG_0^{0.5}(2.67)$ structures.

[g]As in **b**, with $\mathcal{Z} = 1$ and $q = 0.43$.

[h]As in **b**, with $\mathcal{Z} = 1$ and $q = 0.5$.

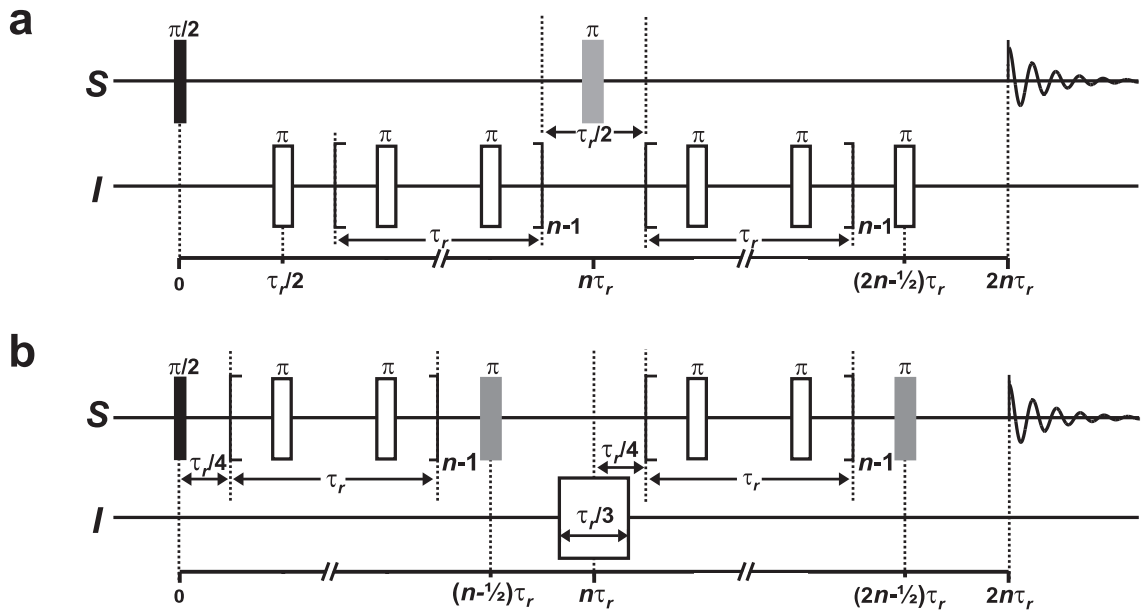


**Figure S1.** Radio-frequency (rf) pulse schemes utilized for acquiring the (a) $^{23}$Na{$^{29}$Si} and $^{23}$Na{$^{31}$P} REDOR,[S28,S29] and (b) $^{29}$Si{$^{23}$Na} and $^{31}$P{$^{23}$Na} REAPDOR[S30] NMR data. For spin-pairs involving a quadrupolar nucleus (here the spin-3/2 $^{23}$Na), coupled to a spin-1/2 I={$^{31}$P, $^{29}$Si} species, one must ensure that the recoupling pulses are applied to the latter for avoiding a severely compromised recoupling performance and NMR signal losses.[S3,S30] Solid black rectangles and open/gray rectangles represent $\pi/2$ and $\pi$-pulses, respectively. The gray rectangles mark pulses with fixed positions, regardless of the choice of the duration of the recoupling period; they are responsible for refocusing S-spin isotropic chemical shifts. The number of recoupling $\pi$-pulses (open rectangles) is incremented in blocks of 4 pulses that together span two rotational periods. This is commensurate with $\tau_{\mathrm{rec}} = 2n\tau_r$ and $n = 1, 2, 3, \ldots$. The reference signal $S_0(\tau_{\mathrm{rec}})$ in (a) is recorded by leaving out all I-spin recoupling pulses, whereas $S_0(\tau_{\mathrm{rec}})$ in (b) results by only omitting the I-spin adiabatic-passage pulse.

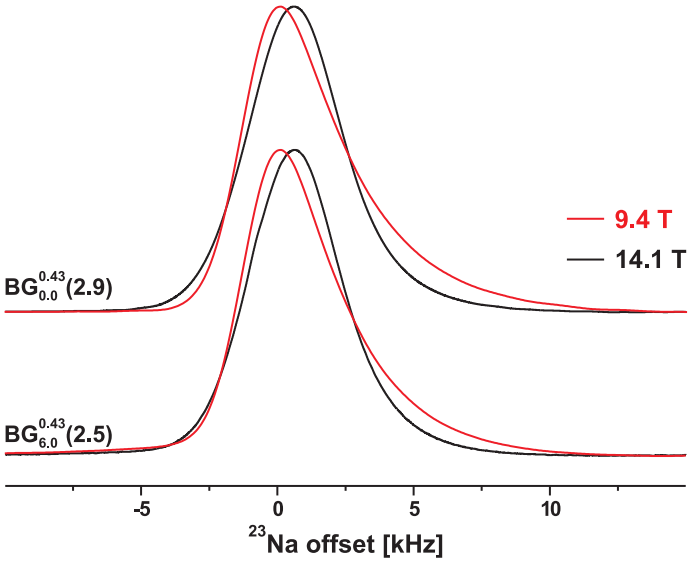


**Figure S2.** $^{23}$Na MAS spectra recorded at external fields of $B_0$=9.4 T and $B_0$=14.1 T at the MAS rates of 14.0 and 24.0 kHz, respectively. Note the very similar fwhm peak-widths observed from each glass at both $B_0$ values, indicating that the emphasized second-order quadrupolar peak-broadening (that scales as $B_0^{-1}$) resulting at the lower field is counterbalanced nearly exactly by the reduced chemical-shift dispersion (scaling linearly with $B_0$). The main distinctions among the NMR spectra are manifested in their shifted peak-maxima and the more pronounced tail towards lower ppm-values observed at $B_0$=9.4 T, both stemming from the larger second-order quadrupolar effects at the lower field.

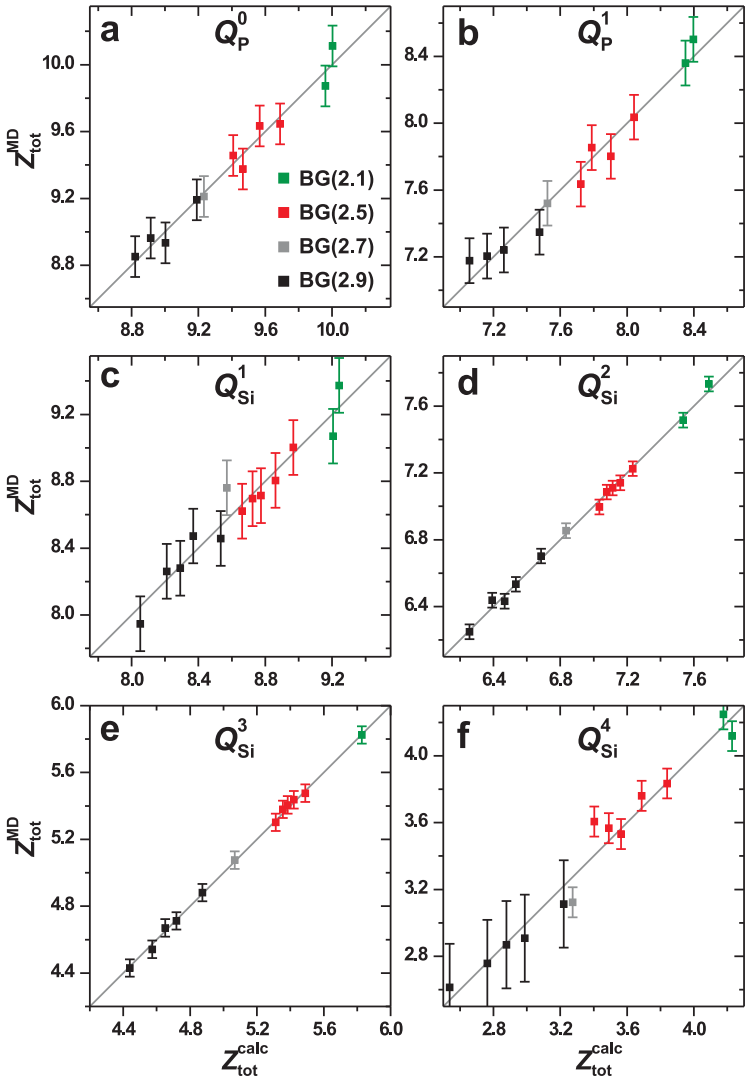


**Figure S3.** Correlation between the MD-derived total coordination number $Z_{\mathrm{tot}}^{\mathrm{MD}}$ and its modeled counterpart $Z_{\mathrm{tot}}^{\mathrm{calc}}$ calculated from eqs. (S1)–(S6) for the as-indicated $Q_T^n$ groups. Each straight line of unity slope marks the ideal correlation.

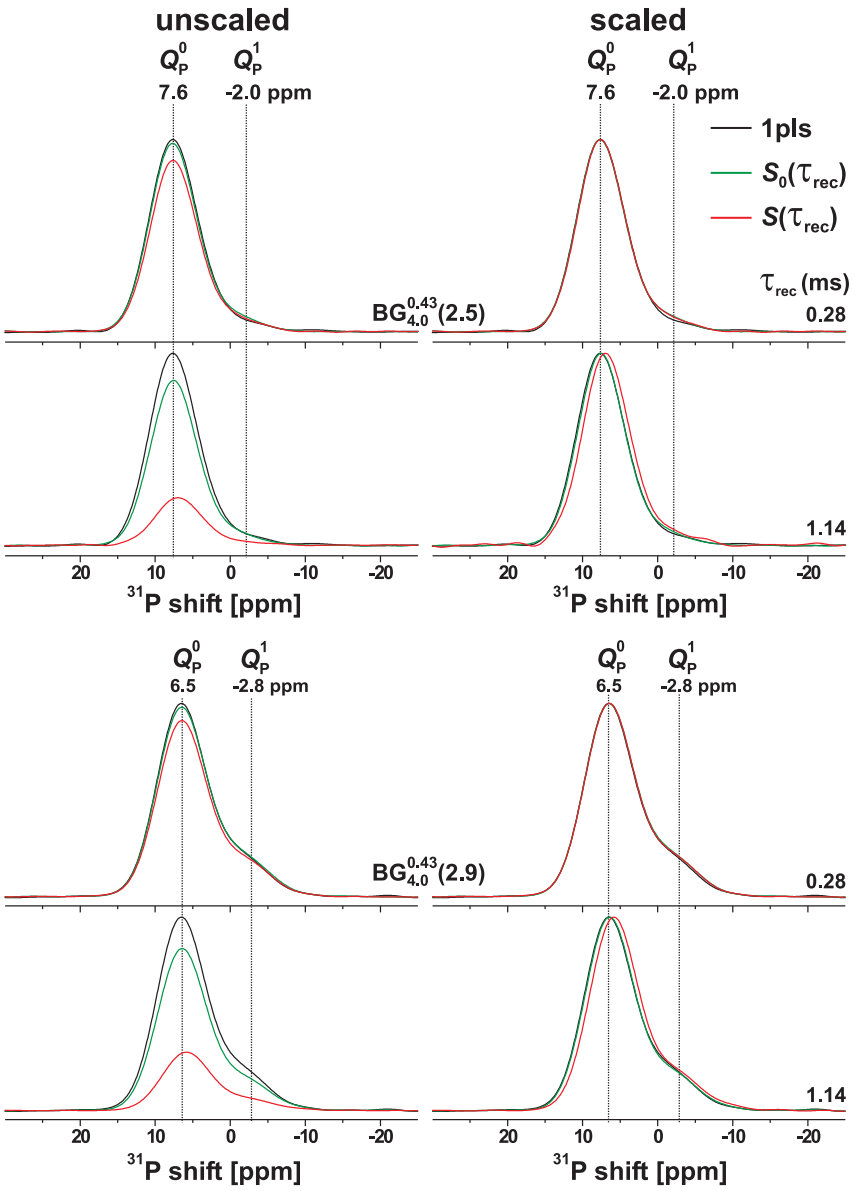


**Figure S4.** $^{31}$P MAS NMR spectra recorded either by direct excitation using single pulses ("1pls") or by $^{31}$P{$^{23}$Na} NMR REAPDOR, where $S(\tau_{\mathrm{rec}})$ and $S_0(\tau_{\mathrm{rec}})$ represents the spectrum obtained in the *presence* and *absence* of dipolar dephasing, respectively (see Fig. **S1**). Data from two dephasing periods of $\tau_{\mathrm{rec}} = 0.28$ ms and $\tau_{\mathrm{rec}} = 1.14$ ms are displayed for each as-indicated $\mathrm{BG}_p^q(\overline{N}_{\mathrm{BO}}^{\mathrm{Si}})$ specimen, with the left and right columns presenting NMR spectra using absolute and relative NMR peak intensities, respectively. The NMR peak positions from the $Q_{\mathrm{P}}^0$ and $Q_{\mathrm{P}}^1$ groups are indicated. All phosphate moieties exhibit an overall similar dipolar dephasing: this effect stems from a slightly larger coordination number $Z_{\mathrm{Na}}(Q_{\mathrm{P}}^0)$ of the $Q_{\mathrm{P}}^0$ groups compared with that of the $Q_{\mathrm{P}}^1$ groups, $Z_{\mathrm{Na}}(Q_{\mathrm{P}}^1)$ (see Fig. **9**), *despite* that the latter displays a higher *preference* for contacts with Na relative to Ca. The resulting (slightly) higher dipolar second moment $M_2(Q_{\mathrm{P}}^0\text{–Na})$ is reflected in the depleted NMR signal intensity at high ppm-values and an accompanying NMR peak-displacement of the $^{31}$P NMR signal from $Q_{\mathrm{P}}^0$ groups towards lower shifts in the REAPDOR-dephased NMR spectrum $[S(\tau_{\mathrm{rec}})]$ relative to its "reference"counterpart $[S_0(\tau_{\mathrm{rec}})]$. This trend is observed for both BG specimens.

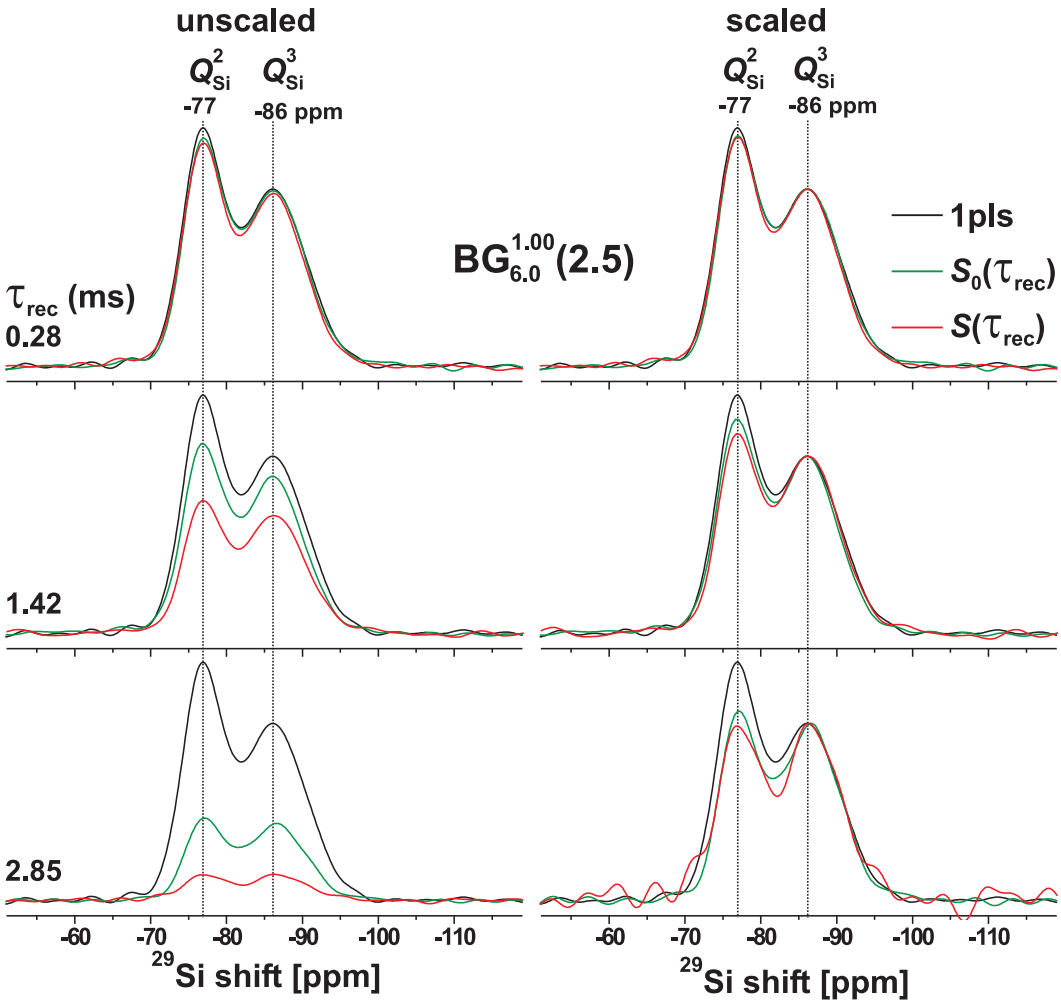


**Figure S5.** $^{29}$Si MAS NMR spectra recorded from the $BG^{1.00}_{6.0}(2.5)$ glass, either by using single pulses ("1pls") or $^{29}$Si{$^{23}$Na} REAPDOR NMR with increasing dephasing intervals $\tau_{rec}$. All spectra reveal two main $^{29}$Si NMR signals from $Q^2_{Si}$ and $Q^3_{Si}$ structural moieties. The higher dipolar dephasing observed from the $Q^2_{Si}$ groups compared with their $Q^3_{Si}$ counterparts is consistent with $Z_{Na}(Q^2_{Si}) > Z_{Na}(Q^3_{Si})$, *despite* the stronger (relative) preference for the $Q^3_{Si}$ moieties to coordinate Na rather than Ca (see Fig. **9** and **Table S5**). Note that the differences between the black and green curves stem from $T_2$ relaxation effects and rf-pulse imperfections, while the differences between the green and red curves faithfully reflect the various distinct $Q^n_{Si}$–Na contacts.

## References


(S1) Mathew, R.; Stevensson, B.; Tilocca, A.; Edén, M. Toward a Rational Design of Bioactive Glasses with Optimal Structural Features: Composition-Structure Correlations Unveiled by Solid-State NMR and MD Simulations. *J. Phys. Chem. B* **2014**, *118*, 833–844.

(S2) Stevensson, B.; Mathew, R.; Edén, M. Assessing the Phosphate Distribution in Bioactive Phosphosilicate Glasses by $^{31}$P Solid-State NMR and MD Simulations. *J. Phys. Chem. B* **2014**, *118*, 8863–8876.

(S3) Stevensson, B.; Mathew, R.; Yu, Y.; Edén, M. Two Heteronuclear Dipolar Results at the Price of One: Quantifying Na/P Contacts in Phosphosilicate Glasses and Biomimetic Hydroxy-Apatite. *J. Magn. Reson.* **2015**, *251*, 52–56.

(S4) Tilocca, A.; Cormack, A. N. Structural Effects of Phosphorus Inclusion in Bioactive Silicate Glasses. *J. Phys. Chem. B* **2007**, *111*, 14256–14264.

(S5) Sanders, M. J.; Leslie, M.; Catlow, C. R. A. Interatomic Potentials for $SiO_2$. *J. Chem. Soc., Chem. Commun.* **1984**, 1271–1273.

(S6) Tilocca, A.; de Leeuw, N. H.; Cormack, A. N. Shell-Model Molecular Dynamics Calculations of Modified Silicate Glasses. *Phys. Rev. B* **2006**, *73*, 104209.

(S7) Tilocca, A.; Cormack, A. N.; de Leeuw, N. H. The Structure of Bioactive Silicate Glasses: New Insights from Molecular Dynamics Simulations. *Chem. Mater.* **2007**, *19*, 95–103.

(S8) Todorov, I. T.; Smith, W.; Trachenko, K.; Dove, M. T. DL_POLY_3: New Dimensions in Molecular Dynamics Simulations via Massive Parallelism. *J. Mater. Chem.* **2006**, *16*, 1911–1918.

(S9) Gullion, T.; Baker, D. B.; Conradi, M. S. New, Compensated Carr-Purcell Sequences. *J. Magn. Reson.* **1990**, *89*, 479–484.

(S10) Yao, Z.; Kwak, H.-T.; Sakellariou, D.; Emsley, L.; Grandinetti, P. J. Sensitivity Enhancement of the Central Transition NMR Signal of Quadrupolar Nuclei Under Magic-Angle Spinning. *Chem. Phys. Lett.* **2000**, *327*, 85–90.

(S11) Chan, J. C. C.; Eckert, H. Dipolar Coupling Information in Multispin Systems: Application of a Compensated REDOR NMR Approach to Inorganic Phosphates. *J. Magn. Reson.* **2000**, *147*, 170–178.

(S12) Nishimura, K.; Fu, R.; Cross, T. A. The Effect of RF Inhomogeneity on Heteronuclear Dipolar Recoupling in Solid State NMR: Practical Performance of SFAM and REDOR. *J. Magn. Reson.* **2001**, *152*, 227–233.

(S13) Gullion, T.; Vega, A. J. Measuring Heteronuclear Dipolar Couplings for I=1/2, S>1/2 Spin Pairs by REDOR and REAPDOR NMR. *Prog. NMR Spectrosc.* **2005**, *47*, 123–136.

(S14) Gan, Z. Rotary Resonance Echo Double Resonance for Measuring Heteronuclear Dipolar Coupling under MAS. *J. Magn. Reson.* **2006**, *183*, 247–253.

(S15) Yap, A. T-W.; Förster, H.; Elliott, S. R. Spin-Echo Double Resonance NMR Evidence for Preferential Like-Cation Clustering in Mixed-Alkali Disilicate Glasses. *Phys. Rev. Lett.* **1995**, *75*, 3946–3949.

(S16) Gee, B.; Eckert, H. Cation Distribution in Mixed-Alkali Silicate Glasses. NMR Studies by $^{23}$Na-{$^{7}$Li} and $^{23}$Na-{$^{6}$Li} Spin Echo Double Resonance. *J. Phys. Chem.* **1996**, *100*, 3705–3712.

(S17) Ratai, E.; Janssen, M.; Eckert, H. Spatial Distributions and Chemical Environments of Cations in Single- and Mixed Alkali Borate Glasses: Evidence from Solid State NMR. *Solid State Ionics* **1998**, *105*, 25–37.

(S18) Bertmer, M.; Eckert, H. Dephasing of Spin Echoes by Multiple Heteronuclear Dipolar Interactions in Rotational Echo Double Resonance NMR Experiments. *Solid State Nucl. Magn. Reson.* **1999**, *15*, 139–152.

(S19) Ratai, E.; Chan, J. C. C.; Eckert, H. Local Coordination and Spatial Distribution of Cations in Mixed-Alkali Borate Glasses. *Phys. Chem. Chem. Phys.* **2002**, *4*, 3198–3208.

(S20) Strojek, W.; Kalwei, M.; Eckert, H. Dipolar NMR Strategies for Multispin Systems Involving Quadrupolar Nuclei: $^{31}$P{$^{23}$Na} Rotational Echo Double Resonance (REDOR) of Crystalline Sodium Phosphates and Phosphate Glasses. *J. Phys. Chem. B* **2004**, *108*, 7061–7073.

(S21) Eckert, H.; Elbers, S.; Epping, J. D.; Janssen, M.; Kalwei, M.; Strojek, W.; Voigt, U. Dipolar Solid State NMR Approaches Towards Medium-Range Structure in Oxide Glasses. *Topics Curr. Chem.* **2005**, *246*, 195–233.

(S22) Tsuchida, J.; Schneider, J.; Orlandi de Oliveira, A.; Rinke, M. T.; Eckert, H. Sodium Distribution in Mixed Alkali K-Na Metaphosphate Glasses. *Phys. Chem. Chem. Phys.* **2010**, *12*, 2879–2887.

(S23) Florian, P.; Vermillion, K. E.; Grandinetti, P. J.; Farnan, I.; Stebbins, J. F. Cation Distribution in Mixed Alkali Disilicate Glasses. *J. Am. Chem. Soc.* **1996**, *118*, 3493–3497.

(S24) Lee, S. K.; Stebbins, J. F. Nature of Cation Mixing and Ordering in Na-Ca Silicate Glasses and Melts. *J. Phys. Chem. B* **2003**, *107*, 3141–3148.

(S25) Lee, S. K.; Mysen, B. O.; Cody, G. D. Chemical Order in Mixed-Cation Silicate Glasses and Melts. *Phys. Rev. B* **2003**, *68*, 2142061–2142067.

(S26) Czjzek, G.; Fink, J.; Götz, F.; Schmidt, H.; Coey, J. M. D.; Rebouillat, J.-P.; Liénard, A. Atomic Coordinataion and the Distribution of Electric Field Gradients in Amorphous Solids. *Phys. Rev. B* **1981**, *23*, 2513–2530.

(S27) Pedone, A.; Gambuzzi, E.; Menziani, M. C. Unambiguous Description of the Oxygen Environment in Multicomponent Aluminosilicate Glasses from $^{17}$O Solid State NMR Computational Spectroscopy. *J. Phys. Chem. C* **2012**, *116*, 14599–14609.

(S28) Gullion, T.; Schaefer, J. Rotational-Echo Double-Resonance NMR. *J. Magn. Reson.* **1989**, *81*, 196–200.

(S29) Gullion, T.; Schaefer, J. Detection of Weak Heteronuclear Dipolar Coupling by Rotational-Echo Double-Resonance Nuclear Magnetic Resonance. *Adv. Magn. Reson.* **1989**, *13*, 57–83.

(S30) Gullion, T. Measurement of Dipolar Interactions between Spin-1/2 and Quadrupolar Nuclei by Rotational-Echo, Adiabatic-Passage, Double-Resonance NMR. *Chem. Phys. Lett.* **1995**, *246*, 325–330.